



Using geostatistical method to delimit a water bearing formations

L. Ouadif*, L. Bahi, K. Baba

3GIE Laboratory, Mohammadia Engineering School, Mohammed V University, Rabat, Morocco

Received 27 July 2014; Revised 4 October 2014; Accepted 8 October 2014.

**Corresponding Author. E-mail: ouadif@gmail.com; Tel: (+2120664451804)*

Abstract

Morocco is a country which has semi-arid to arid climate. Rainfall is irregular in time and space. Surface water undergoes very large fluctuations according to variation of the hydraulicity during all the year. The groundwater resources play a very important role in supplying water to rural populations and irrigation. The purpose of this study was the evaluation of geostatistical methods for delimitation of water-bearing formations in Outita region. Thus a geophysical survey of 52 geoelectric soundings VES was performed with a mesh of 500 m using the Schlumberger array with current electrodes spacings between 200 and 3000 m. Geostatistical tools were used to quantify the spatial correlation between apparent resistivity data. Semivariograms were obtained using a classical Matheron semivariogram estimator and fitted to the obtained experimental semivariograms. We have selected those with the best fit in terms of sum of squared residuals (SSR). The structural analysis is based on the study of oil drillings. It shows that the Jurassic and Neogene formations are affected by normal and reverse faults delimiting horsts and grabens. The qualitative interpretation of the kriged resistivity maps allows defining resistivity contrast; consequently we have delimited water-bearing formations. The resistivity maps confirmed the graben structure, obtained from the structural analysis, with NW SE direction. Models of the geology were successfully obtained from geostatistical method, which help mapping the water-bearing formations and the estimations of groundwater resources.

Keywords: Groundwater, Geoelectric prospecting, Geostatistical Interpolation, Kriging

Introduction

In order to identify and characterize formations that may be potential aquifers to fulfil the increased water requirements of the rural population for drinking and irrigation in Outita plain (Fig.1), geophysical data produced in the area have been interpreted. This region is part of Gharb basin which is bounded on the north by the Préfif, on the east by the préfifaines ridges, on the south by the Moroccan Meseta and on the West by the Atlantic Ocean.

The Gharb basin knew many subsidences during certain periods, with a paroxysm in the Pliocene [1, 2]. The former works reflect the structural complexity of Gharb basin in general and particularly its eastern boundary. Thus, it is necessary to conduct synthetic studies implying local geology, study of oil drillings and interpretation of all carried out geoelectric soundings.

Our study begins with a statistical analysis of the 52 electrical soundings that are realized. Then we calculate and model experimental variograms for each level AB using VarioWin 2.2® software. Isoresistivity maps were produced using ordinary kriging of Geostatistical Analyst® (extension ArcGIS 9.3™).

2. Materials and methods

2.1. Data acquisition

The electrical resistivity method is most used in engineering geology. It identifies and locates, from the earth surface, the structures which have resistivity contrasts [4, 5, 6, 7]. It consists of conducting geoelectric sounding to determine, at several points, the vertical succession of layers of different resistivity. This method is based on the principle of Ohm's law: the injection in soil of a direct current at a very low frequency and then voltage measurement makes it possible to unveil the true resistivity of crossed formations. Several devices were used among which the most known is the Schlumberger one. In this device (Figure 2), we inject a current into two electrodes A and B, and we measure the voltage at the receiving electrodes M and N. Apparent resistivity is given by:

$$\rho_{app} = \pi \frac{(L^2 - l^2)}{2l} \frac{\Delta V}{I} \quad \text{or} \quad \rho_{app} = K \frac{\Delta V}{I} \quad (1)$$

where K is the geometric factor that depends on electrodes spacing only.

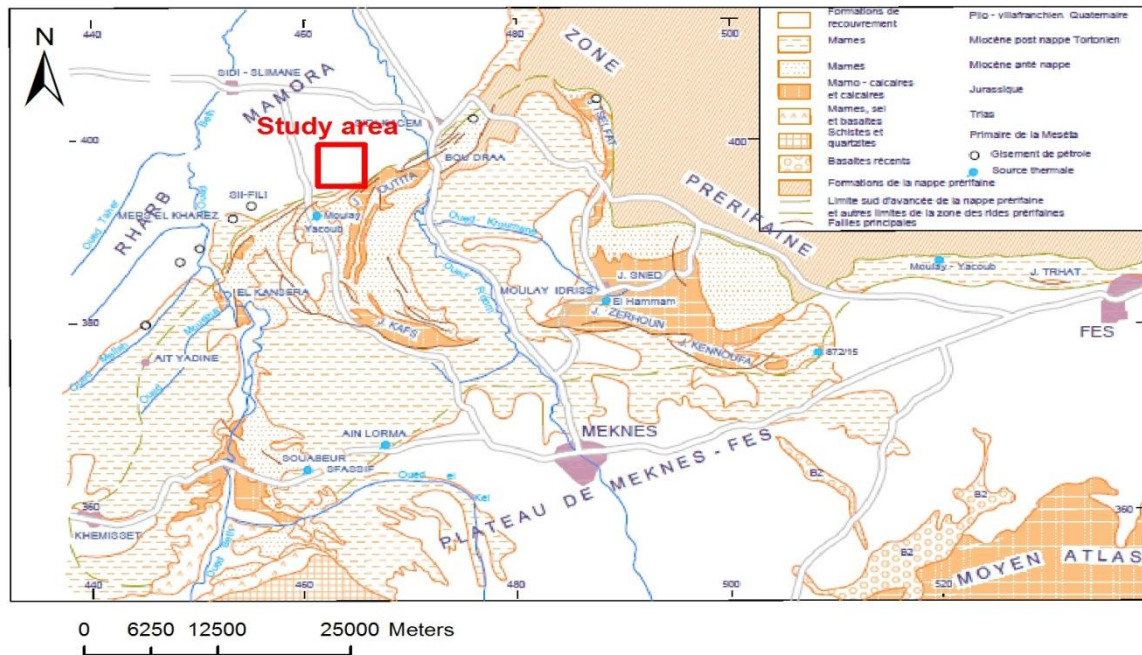


Figure 1. Geographical and geological situation of the study area [3]

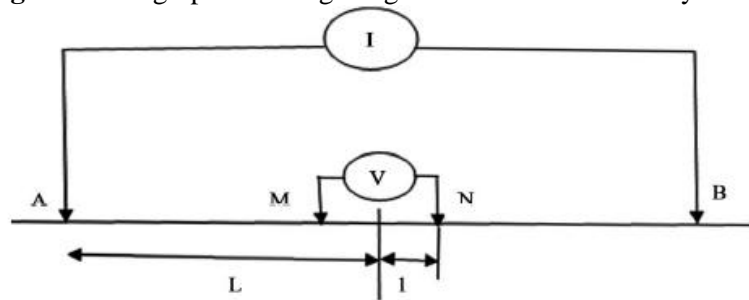


Figure 2. Schlumberger array.

Our geophysical survey covers an area of 20 km² and includes 52 geoelectric soundings (figure 3). Resistivity measurements were made at nodes of a more or less regular square grid. The size of the mesh is approximately 500m. VES were carried out using Schlumberger array, the distances between current electrodes being systematically 200, 400,600,800,1000,1400,2000 and 3000m [8, 9]. Our goal is to develop a method to generate pertinent 2D resistivity models in order to determine the vertical and lateral extents of water-bearing formations.

2.2. Geostatistics

Geostatistics, started with the work in geology and mining of Krige [10] then developed by Matheron [11] with his theory of regionalized variables, are methods of interpolation which predict unknown values from data observed at known locations, and it minimizes the error of predicted values which are estimated by spatial distribution of the predicted values. As variables are supposed having an effect on each other, the first concept is related to the variogram of values we want to estimate. It relates the similarity or difference, expressed as the semi-variance, between values at different places to their separation distance (lag) and direction. Distance that variables have an effect on each other is called range of a variogram and is an important concept because after that distance, variables have no effect on each other. The plot of the semivariance versus the lag h is called semivariogram (figure 4). In some cases, it increases with h and reaches an asymptotic value, a sill. Range is the value of h at which the semivariogram asymptotes. Values of the properties at sites separated by a distance shorter than the range will be spatially correlated. The range depends on the scale of the study and on the property evaluated.

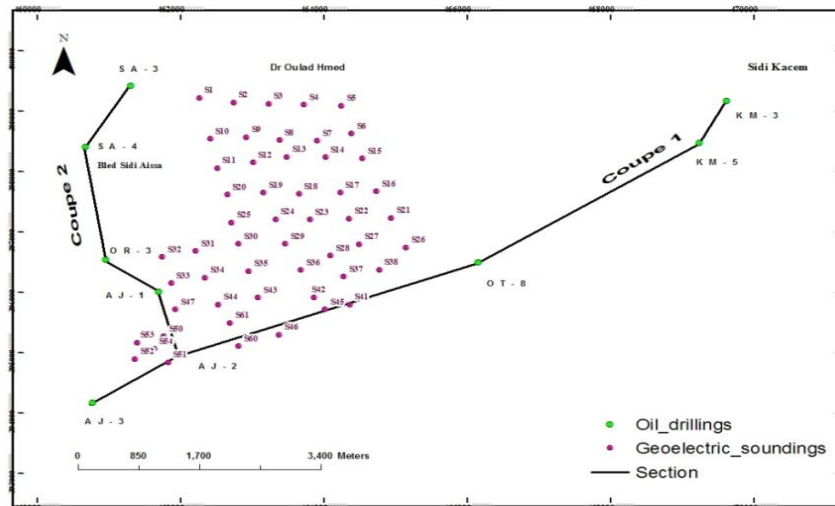


Figure 3. Location map of geoelectric soundings

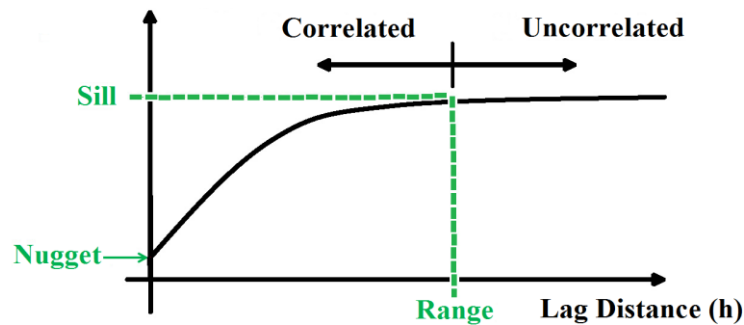


Figure 4. Semivariogram model parameters

The technique of variogram (or semi-variogram) quantifies the spatial variability of a regionalized variable, and provides the input parameters for the spatial interpolation of kriging [10, 12].

Let be $\rho(x)$ and $\rho(x+h)$ the values of electrical resistivity sampled at positions x and $x+h$, with h a distance, known as lag, which separates both positions, semi-variances can be estimated as [10, 11]:

$$\gamma(h) = \frac{1}{2} E[\rho(x) - \rho(x+h)]^2 \quad (2)$$

For discrete sampling sites, such as earthen material samples, the function is estimated as:

$$\gamma(h) = \frac{1}{2N(h)} \sum_{i=1}^{N(h)} [\rho(x_i) - \rho(x_i+h)]^2 \quad (3)$$

Where $\rho(x_i)$: the value of electrical resistivity ρ at location of x_i

$N(h)$: the number of point pairs for distance class h .

The five models most frequently used are:

$$\text{Nugget: } g(h) = \begin{cases} 0 & \text{if } h=0 \\ c & \text{otherwise} \end{cases} \quad (4)$$

$$\text{Spherical: } g(h) = \begin{cases} c \cdot \left(1.5 \left(\frac{h}{a}\right) - 0.5 \left(\frac{h}{a}\right)^3\right) & \text{if } h \leq a \\ c & \text{otherwise} \end{cases} \quad (5)$$

$$\text{Exponential: } g(h) = c \cdot \left(1 - \exp\left(\frac{-3h}{a}\right)\right) \quad (6)$$

$$\text{Gaussian: } g(h) = c \cdot \left(1 - \exp\left(\frac{-3h^2}{a^2}\right)\right) \quad (7)$$

$$\text{Power: } g(h) = c \cdot h^w \quad 0 < w < 2 \quad (8)$$

With h : lag distance
 c : sill
 a : range

Nugget effect is essential to optimize the process under study: the higher its difference for the semivariogram sill, the higher the phenomenon continuity, the lower the estimation variance, or the higher the estimation confidence. The variogram plot is fitted with a theoretical model which provides information about the spatial structure as well as the input parameters for kriging interpolation. Kriging algorithms [10] are described as a best linear unbiased estimator (BLUE), which is a process of a theoretical weighted moving average:

$$\rho(x_0) = \sum_{i=1}^n \lambda_i \rho(x_i) \quad (9)$$

Where $\rho(x_0)$ is the value to be estimated at the location of x_0 , $\rho(x_i)$ is the known value at the sampling site x_i . And λ_i denotes the weight of the i th observation, they are calculated searching an unbiased estimator of z with minimum variance [13].

The estimation errors (or kriging variances) need to be minimized. To ensure that the estimate is unbiased, the weights need to sum to one:

$$\sum_{i=1}^n \lambda_i = 1 \quad (10)$$

3. Results and discussion

3.1. Geological framework and methodology of work

The Neogene basin of the Gharb is deformed at its borders due to the tectonic movements of the Prerif and prerifaines ridges [14, 15]. The structural analysis is based on the study of oil drillings. North East-South West correlations drillings show that the Jurassic and Neogene formations are affected by normal faults which cause a collapse of both sides of an upper area formed by Jurassic deposits (boreholes OT8 and KM5) with thickening of the Miocene, and reverse faults that delimit tectonic slices. These reverse faults are mainly due to tension caused by the advance of the prerifaine nappe in the Neogene Gharb basin. However the geoelectric soundings show the heterogeneity of formations met in the south-east Jurassic ridge, which demonstrates the complexity of this area which is affected by normal and reverse faults delimiting horsts and grabens (Figure 5).

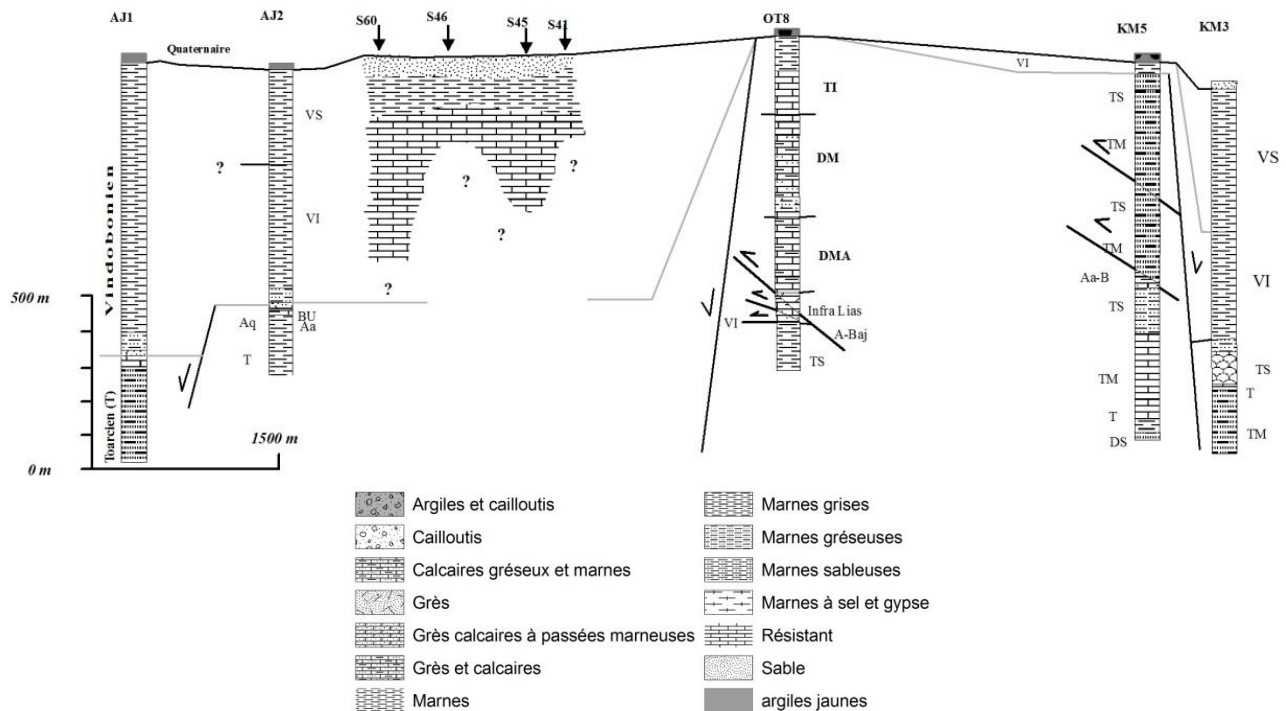


Figure 5. North East-South West geological and geoelectric sections[8]

The North-South correlations, also show a thickening of the Miocene at the areas of collapse that is progressive from Outita link in South towards North in direction of center of Gharb basin. Reverse faults affecting the prerifaine nappe and Miocene deposits result from the deformation caused by the advance of the prerifaine nappe in Gharb basin (Figure 6).

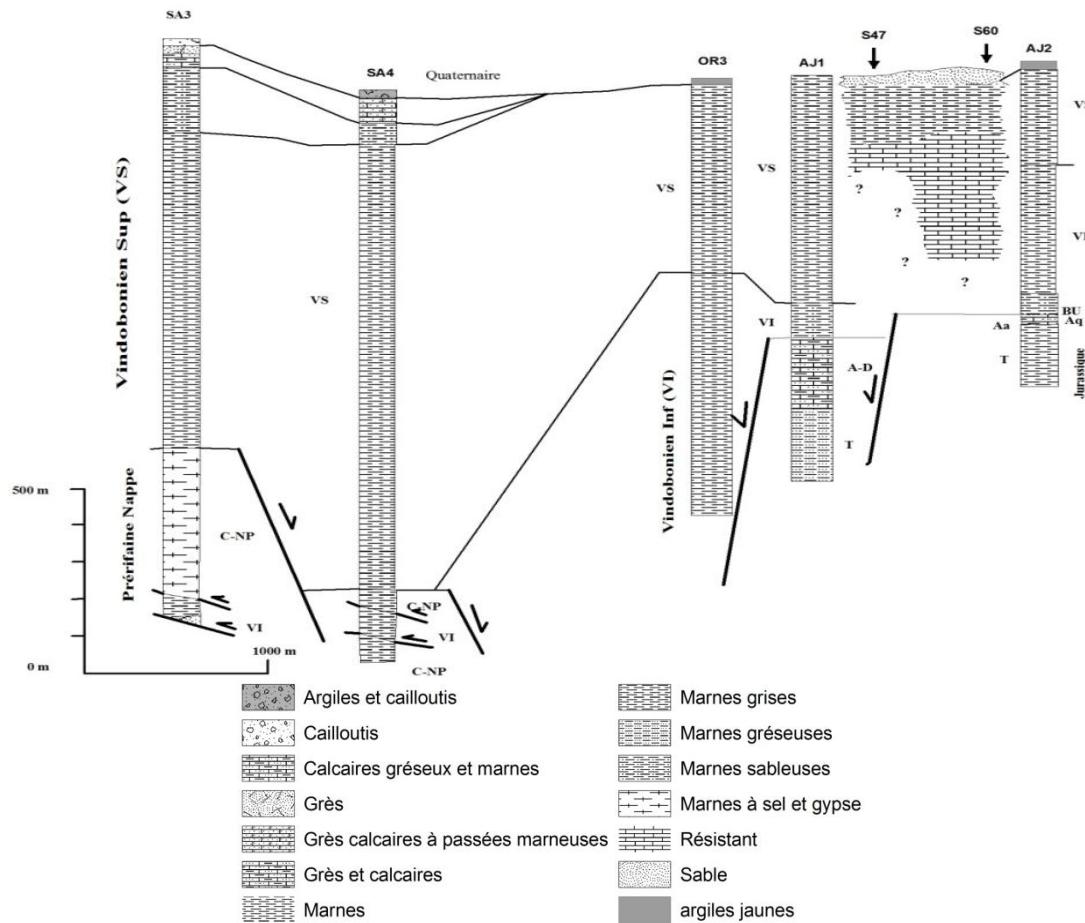


Figure 6. North South geological and geoelectric sections [8].

3.2. Statistical Analysis

The classical statistical procedures assume that variations are randomly distributed within each class of observations and independent of sample location [16] table 1). The mean is therefore used for the estimation of properties for unsampled locations within each class. Statistics of dispersion (e.g. variance, standard deviation, coefficient of variability, confidence limits) are used to show the precision of the mean as an estimator.

Table 1. Summary statistics of random samples

Statistic	Number of samples	Mean	Confidence	Sum	Minimum	Maximum	Variance	Std.Dev.
AB200	52	14,71	11,87	764,80	4,30	48,00	104,05	10,20
AB300	52	14,11	11,21	733,60	3,60	51,00	108,69	10,43
AB400	52	13,58	10,66	706,10	2,60	51,00	110,01	10,49
AB600	52	8,22	6,39	427,40	2,40	35,00	43,01	6,56
AB800	52	7,24	5,76	376,70	1,70	29,00	28,31	5,32
AB1000	52	7,60	6,28	395,30	1,30	26,00	22,40	4,73
AB1400	52	7,63	6,83	396,56	2,60	19,00	8,10	2,85
AB2000	52	12,78	11,99	664,78	7,00	20,00	8,12	2,85
AB3000	52	15,79	13,93	821,11	5,32	35,00	44,74	6,69

Assuming the samples were collected randomly from different locations in the field, we can conclude from these statistics that resistivity at the upper sublayers is more variable on the field than that at the lower layers.

3.3. Geostatistical methods

We calculate experimental electrical resistivity semivariograms of experimental fields in order to obtain the parameters: range, sill and nugget variance for evaluating the spatial correlation of these variables (figure 7). Semivariograms were obtained using a classical Matheron semivariogram estimator.

The experimental semivariograms were fitted with various theoretical models like spherical, exponential, gaussian, linear and power by an automatic (least-squares) estimation of semivariogram parameters. Indicator variograms were built adopting a lag of 300 m. The theoretical model that gave minimum standard error is chosen for further analysis. The models adopted are the Gaussian, the spherical and the exponential models. Their parameters are shown in table 2.

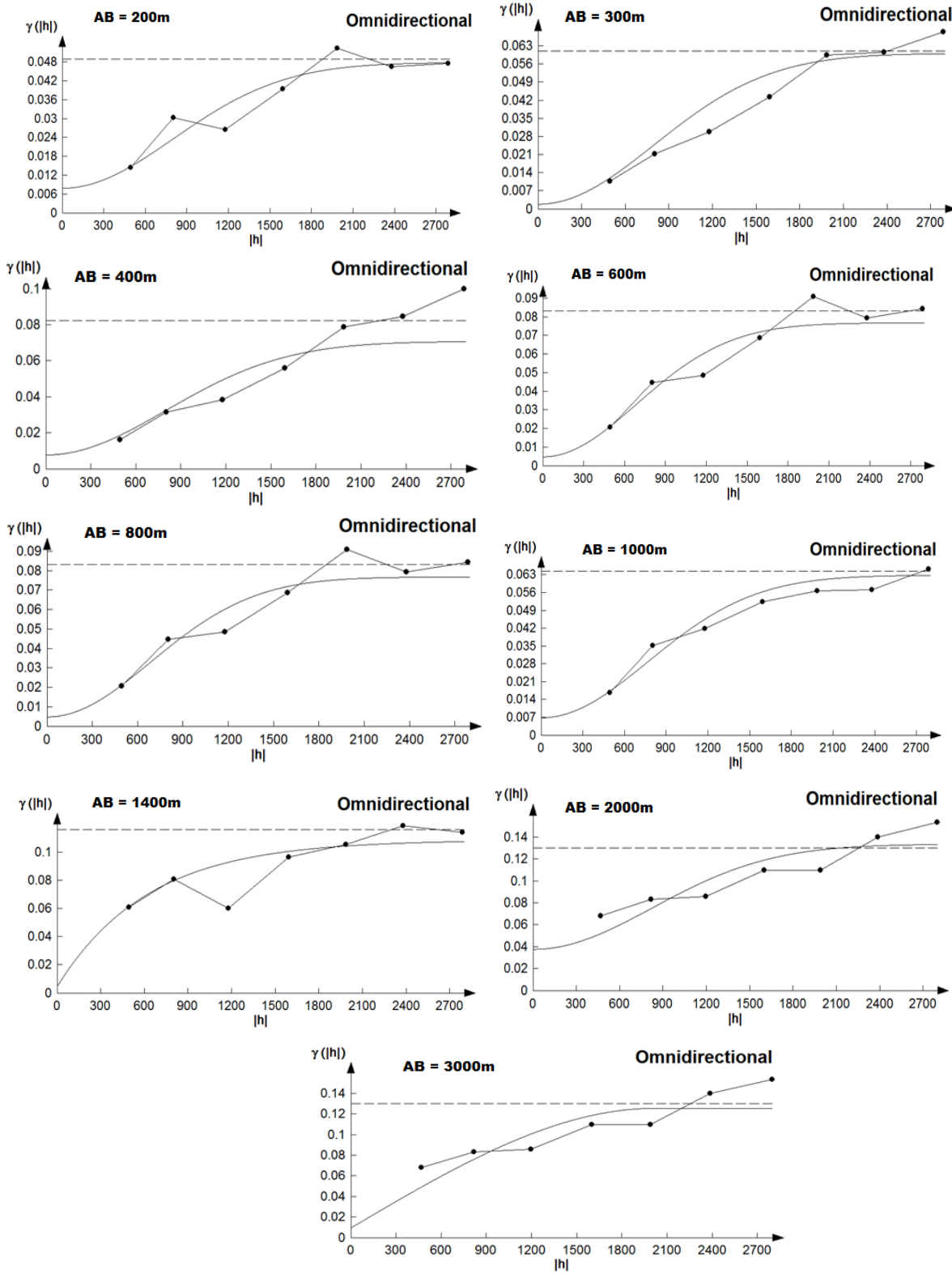


Figure 7. Experimental semivariogram and fitted models for each AB

Table 2. Semivariogram models parameters

	Model	Nugget	Range (m)	Sill
AB = 200m	Gaussien	0.008	1960	0.048
AB = 300m	Gaussien	0.002	1950	0.058
AB = 400m	Gaussien	0.008	1960	0.063
AB = 600m	Gaussien	0.002	1700	0.088
AB = 800m	Gaussien	0.005	1680	0.072
AB = 1000m	Gaussien	0.007	1400	0.056
AB = 1400m	Exponentiel	0.005	1880	0.104
AB = 2000m	Gaussien	0.038	2000	0.096
AB = 3000m	Sphérique	0.01	2000	0.116

Spatial interpolation accuracy and precision were evaluated through cross-validation approach. Most important criteria include: mean bias error (MBE), mean absolute error (MAE), mean squared error (MSE) and root mean squared error (RMSE). MAE and RMSE are among the “best” overall measures of model performance [17]. RMSE provides a measure of error size, but it is sensitive to outliers as it places a lot of weight on large errors. MAE provides an absolute measure of the size of the error, and it is less sensitive to extreme values. The definitions of MAE, MBE and RMSE are as follows:

$$MAE = \frac{1}{n} \sum_{i=1}^n |z^*(x_i) - z(x_i)| \quad (11)$$

$$MBE = \frac{1}{n} \sum_{i=1}^n (z^*(x_i) - z(x_i)) \quad (12)$$

$$RMSE = \sqrt{\frac{1}{n} \sum_{i=1}^n (z^*(x_i) - z(x_i))^2} \quad (13)$$

Cross-validation of the model is shown in figure 8 for each variable AB. The scatter of points is around the 1:1 line, we conclude that the predicted and measured values are almost equals.

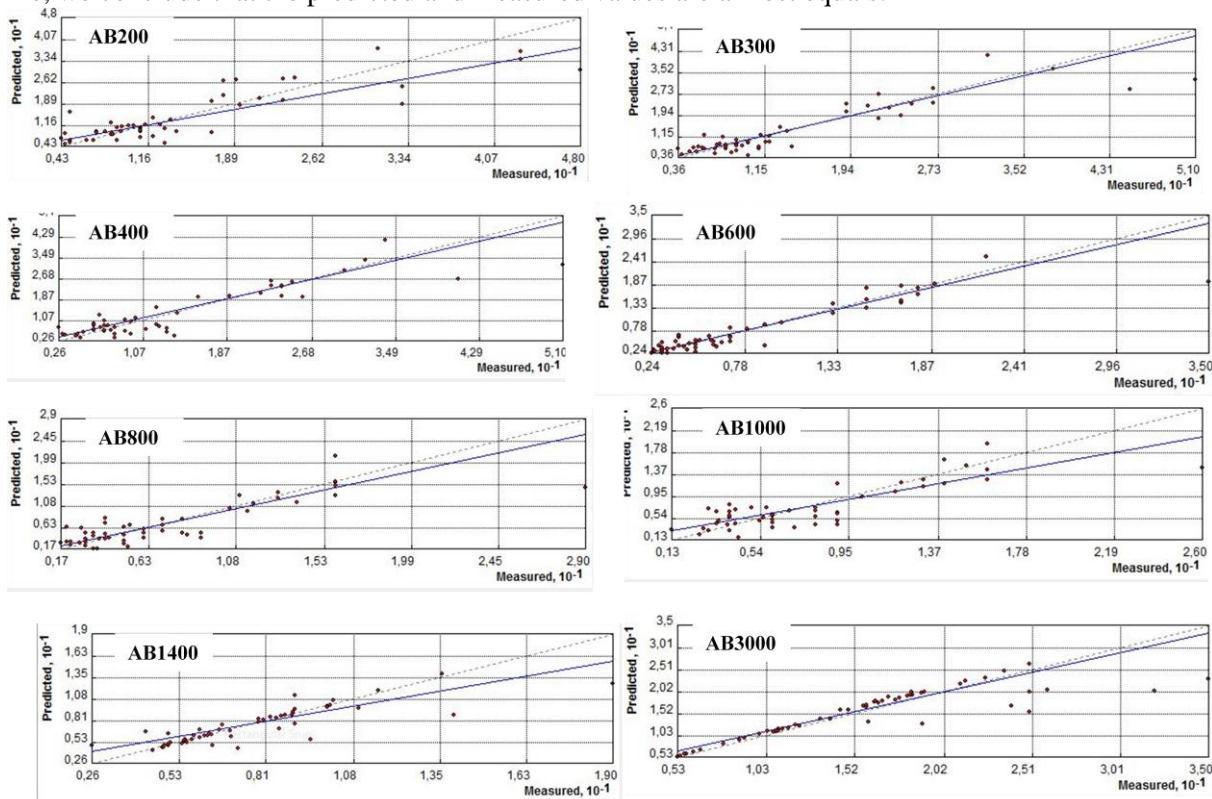


Figure 8: Cross validation graphs for each AB

After analysis of spatial dependence, we use ordinary kriging to estimate unknown values for each level AB. We then produce iso-resistivity maps.

3.3. Results

The apparent resistivity maps (Fig. 9) obtained for different lengths of line AB are similar to two-dimensional electrical cartography. According to [18], the effective depth Z_e is equal to $0.19 * L$ where L is the inter-electrode spacing AB. The following table (table3) shows the different lengths of line AB with the respective effective depths.

Table 3. Electrodes spacing with respective effective depth

AB (m)	200	300	400	600	800	1000	1400	2000	3000
Z_e (m)	38	57	76	114	152	190	266	380	570

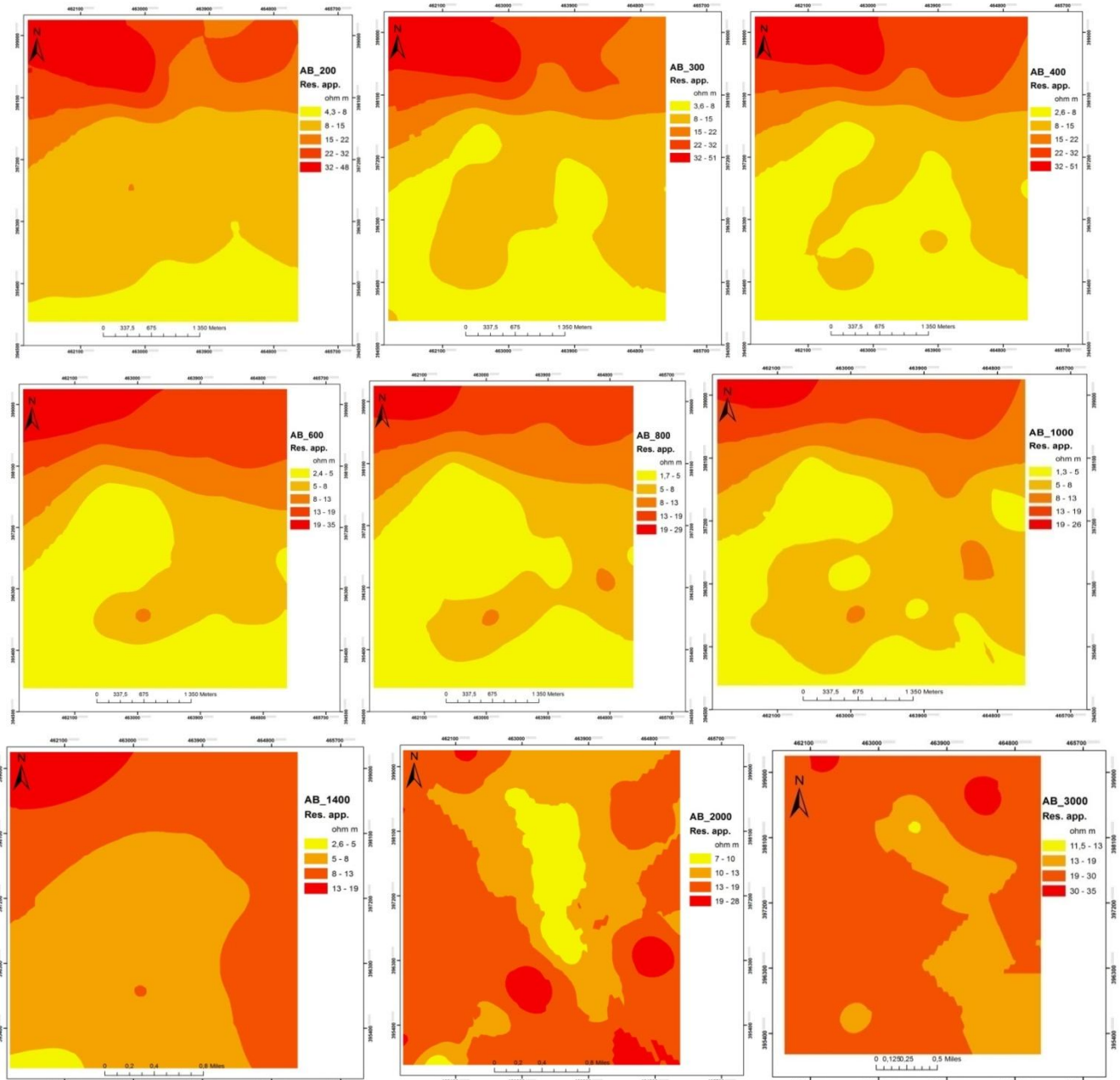


Figure 9. Resistivity maps for each AB

For shallow depths we have resistant formations that correspond to the Plio quaternary complex with conglomerates, sandy marl and marl locally in the south.

More AB increases, more the resistivity decreases highlighting marly formations which extend over most of the area at depths of 50m to 200m ($AB = 300$ to $1000m$). As the depth increases, the apparent resistivity increases on either side of a graben which has a NW / SE direction with marly filling. This agrees with the oil drilling

correlations. The resistant formations situated on either side of that graben are constituted by sandstone which are potentially aquifers and are reached at depths approaching 300m.

Conclusion

Gharb Basin has been the subject of several geological, geophysical and sedimentological studies; however, the eastern boundary of the basin, where is the study area, remains unknown. Oil drillings correlations conducted in Sidi Kacem region show reverse faults affecting the Jurassic and the Neogene due to tension caused by the prerifaine nappe advance.

A geophysical survey of 52 geoelectric soundings VES was performed with a mesh of 500 m using the Schlumberger array with current electrodes spacings between 200 and 3000 m. We use ordinary kriging to estimate unknown values for each electrode spacing AB to produce isoresistivity maps for corresponding effective depth Ze.

The qualitative interpretation of these maps shows that the apparent resistivity increases on either side of a graben which has a NW / SE direction with marly filling. This agrees with the oil drillings correlations. The resistant formations situated on either side of that graben are constituted by sandstone which are potentially aquifers and are reached at depths approaching 300m.

Our results suggest that geostatistical methods are potentially very useful for building a model in the area of complicated geological structures.

References

1. Faugères J. C., Les Rides Sud-Rifaines. Evolution Sédimentaire et Structurale d'un Bassin Atlantico- Mésogéen de la Marge Africaine, Thèse de Doctorat d'Etat, 2 Tomes, Université Bordeaux I, (1978).
2. Litto W., Apport de la Sismique Réflexion et des Diagraphies à l'Etude de l'Evolution Géodynamique D'un Bassin Néogène à Potentiel Pétrolier: Exemple de la Marge Nord du Bassin du Gharb (Avant Pays Rifain, Maroc), Thèse de Doctorat, Faculté des Sciences Rabat, Maroc, (2001).
3. Combe M., La Zone pré-rifaine et les Rides pré-rifaines, Ressources en Eau du Maroc, Tome 1, Editions Du Service Géologique Du Maroc, Rabat, (1971).
4. Chouteau T., Les Méthodes Electriques, Notes de Cours, Publications Ecole Polytechnique, Montréal, (2001).
5. Telford W.M., Geldart L.P., Sheriff R.E., *Applied Geophysics* (1990). Cambridge University Press. 770pp.
6. Baba K., Bahi L., Ouadif L., Akhssas A., Mapping Sterile Bodies in the Sidi Chennane phosphatic deposit (Morocco) using geoelectrical, Investigations, *International Journal of Engineering Research and Applications (IJERA)*, 2 (5) (2012) 2132-2136.
7. Baba K., Bahi L., Ouadif L., Cherradi C., Application des méthodes d'analyses statistiques multivariées à la délimitation des anomalies de Sidi Chennane (Multivariate Statistical Analysis tool for the interpretation of geoelectrical data: application to Sterile Bodies in the Sidi Chennane phosphatic deposit (Morocco)), *J. Mater. Environ. Sci.* 5 (4) (2014) 1005-1012
8. Ouadif L., Bahi L., Akhssas A., Baba K., Menzhi M., Contribution of Geophysics for the Determination of Aquifers with a Case Study, *International Journal of Geosciences*, 3 (1) (2012) 117-125.
9. Ouadif L., Bahi L., Baba K., Identification of formations of soil and subsoil using finite elements Modeling, *MATEC Web of Conferences* 11 (2014) 03003
10. Krige D.G., A statistical approach to some basic mine valuation problems on the Witwatersrand. *J. Chem. Metall. Min. Soc. S.Africa* 52 (6) (1951) 119-139.
11. Matheron G., *Principles of geostatistics. Econ. Geol.* 58 (1963) 1246-1266
12. Webster R., Oliver, M.A., *Geostatistics for Environmental Scientists*, (2001) John Wiley & Sons Ltd, Chichester
13. Webster R., Quantitative spatial analysis of soil in the field, *Advances in Soil Science* 3 (1985) 1-70 Springer-Verlag, New York.
14. Bargach K., Ruano P., Chabli A., Galindo-ZaldiVar J., Chalouan A., Jabloy A., Akil M., Ahmamou M., Sanz De Galdeano C., Benmakhlouf M., Recent Tectonic Deformations and Stresses in the Frontal Part of the Rif Cordillera and the Saiss Basin (Fes and Rabat Regions, Morocco), *Pure and Applied Geophysics*, 161 (3) (2004) 521.
15. Zizi M., Triassic-Jurassic Extensional Systems and Their Neogene Reactivation in Northern Morocco (The Rides Prerifaines and Guercif Basin), Ph.D. Thesis, Rice University, Houston, (1996).
16. Mohmmadi J. *Pedometrics: Spatial Statistics (Geostatistics)*. Pelk Publications, (2006) pp 453.
17. Willmott C.J., Some comments on the evaluation of model performance, *Bull. Am. Meteorol. Soc.* 63 (1982) 1309
18. Edwards L.S., A modified pseudosection for resistivity and IP. *Geophysics*, 42 (5) (1977) 1020-1036.

(2015) ; <http://www.jmaterenvirosci.com>